Supporting Online Materials

For

Effects of sintering temperature on the internal barrier layer capacitor (IBLC) structure in $CaCu_3Ti_4O_{12}$ (CCTO) ceramics

Rainer Schmidt [a,*], Martin Stennett [b], Neil C. Hyatt [b], Jan Pokorny [b,c], Jesús Prado-Gonjal [d], Ming Li [b], Derek C. Sinclair [b]

[a] *Universidad Complutense de Madrid, Dpt. Física Aplicada III, GFMC, Fac. de CC. Físicas, 28040 Madrid, Spain*

[b] *The University of Sheffield, Materials Science and Engineering, Mappin Street, Sheffield S1 3JD, United Kingdom*

[c] *Academy of Sciences of the Czech Republic, Institute of Physics, Na Slovance 2, 182 21 Prague 8, Czech Republic*

[d] *Universidad Complutense de Madrid, Dpt. Química Inorgánica, Facultad de Ciencias Químicas, 28040 Madrid, Spain*

* Corresponding author. Email: rainerxschmidt@googlemail.com

I. Basic principles of impedance spectroscopy and data analysis

Temperature dependent impedance spectroscopy (IS) enables different contributions to the dielectric and resistive properties of condensed matter to be deconvoluted and characterized separately.[1] IS is therefore the method of choice to separately determine and investigate the dielectric properties of GB and bulk regions in electrically inhomogeneous electroceramics such as CCTO.[2] IS experiments consist of a time (t)-dependent alternating voltage signal U of angular frequency ω and amplitude U_0 applied to a sample, and effectively the phase shift δ and amplitude I_0 of the current response signal I are measured.[3]

$$U(\omega, t) = U_0 \cos(\omega t);$$

$$I(\omega, t) = I_0 \cos(\omega t - \delta);$$

Parameters defined by the applied voltage signal are printed in blue, the measured parameters of the current response are in red. The current response of ideal circuit elements is: (1) in-phase with the applied voltage in the case of an ideal resistor R; (2) out-of-phase by $\delta = -\pi/2$ for an ideal capacitor C; and (3) out-of-phase by $\delta = +\pi/2$ for an ideal inductor. All phase angles are time independent for a given frequency which allows the impedance to be defined as a time-independent complex number Z^* ($= Z' + iZ''$).

It has been shown previously that different dielectric relaxation processes detected by IS such as those found at the GB and the bulk regions can, in the simplest case, be described by an RC circuit element consisting of a resistor and capacitor in parallel.[2] The macroscopic impedance is then just the sum of all series RC impedances where each RC element would appear as a separate semicircle in a complex plane plot of Z'' vs Z'. Using an equivalent circuit fitting procedure the

resistivity and dielectric permittivity of each relaxation can be determined. In Fig.1c in the main text an idealized equivalent circuit model is shown for CCTO accounting for the bulk dielectric relaxation (R1,C1) and the GB effect (R2, C2). In reality, the dielectric relaxation processes in CCTO are usually not ideal and can, therefore, not be modeled by ideal RC elements. The addition of a parallel constant-phase-element (CPE) to R1 and C1 can account for the non-ideality of the intrinsic bulk dielectric response in ceramics sintered at 1100 °C.[4] This approach failed here for samples sintered at lower temperatures in the range from 975 to 1050 °C, which has been reported before for Sr-doped CCTO ceramics sintered at 1000 °C.[5] Nevertheless, for the study presented here full information about the bulk resistivity ρ_1, bulk permittivity ε_1 and GB permittivity ε_2 could be obtained from plots of M'' vs f, and ε' vs f.

In the framework of ideal Debye relaxation processes, as described by ideal parallel RC elements, the M'' vs f plot is particularly useful to display bulk relaxation peaks. Whereas Z'' vs f plots pronounce the relaxation peak with the highest resistivity ρ (e.g. the GB relaxation of CCTO), the M'' vs f plots pronounce the smallest permittivity ε (i.e. the bulk relaxation of CCTO). The height of the bulk relaxation peak $M''(f_{max})$ is proportional to the reciprocal of the bulk permittivity ε_1 according to equation SOM1, and the peak position (f_{max}) is given by equation SOM2:

$$M''(f_{max}) = \frac{1}{2\varepsilon_1}; \qquad \text{(SOM1)}$$

$$f_{max} = \frac{1}{2\pi\ \rho_1\varepsilon_0\varepsilon_1}; \qquad \text{(SOM2)}$$

where ε_0 represents the permittivity of vacuum. Equations SOM1 and SOM2 allow the bulk resistivity ρ_1 and bulk permittivity ε_1 to be established from the relaxation peak in the M'' vs f plot. In the case of a non-ideal impedance response the relaxation peak displayed in the M'' vs f plot is broadened though, the peak height is reduced and ε_1 would be therefore over-estimated according to equation (SOM1). The peak frequency f_{max} is unaffected though by relaxation peak broadening (equation SOM2). Therefore, ε_1 was determined directly from the ε' vs f plot (see Fig.1b and Fig.2 in the main text) using the data collected at 50 K, and ρ_1 could then be calculated from equation (SOM2). In Fig.2 in the main text the ε' vs f curves measured at 80 K for the 1100 °C and the 1075 °C sintered pellets do not fully relax towards the bulk plateau at high f. This is the case though for all ε' vs f curves at 50 K (data not shown), where reliable values for the fully relaxed plateau ε_1* could be determined. The value of such high-frequency, low-permittivity bulk plateau ε_1* can be used as a good estimate for the true bulk permittivity ε_1. It has to be noted though that ε_1* formally contains a contribution from the GB permittivity ε_2 and, therefore, for precise bulk ε_1 values a correction of ε_1* for the GB permittivity ε_2 is necessary. If the GB relaxation is described by R2-C2 and the bulk by R1-C1, the value of the high-frequency, low-permittivity plateau ε_1* is given by:

$$\varepsilon_1^* = \frac{\varepsilon_1 \times \varepsilon_2}{\varepsilon_1 + \varepsilon_2}; \qquad \text{(SOM3)}$$

Equation (SOM3) shows that the "true" intrinsic bulk permittivity value ε_1 may be larger than ε_1*.

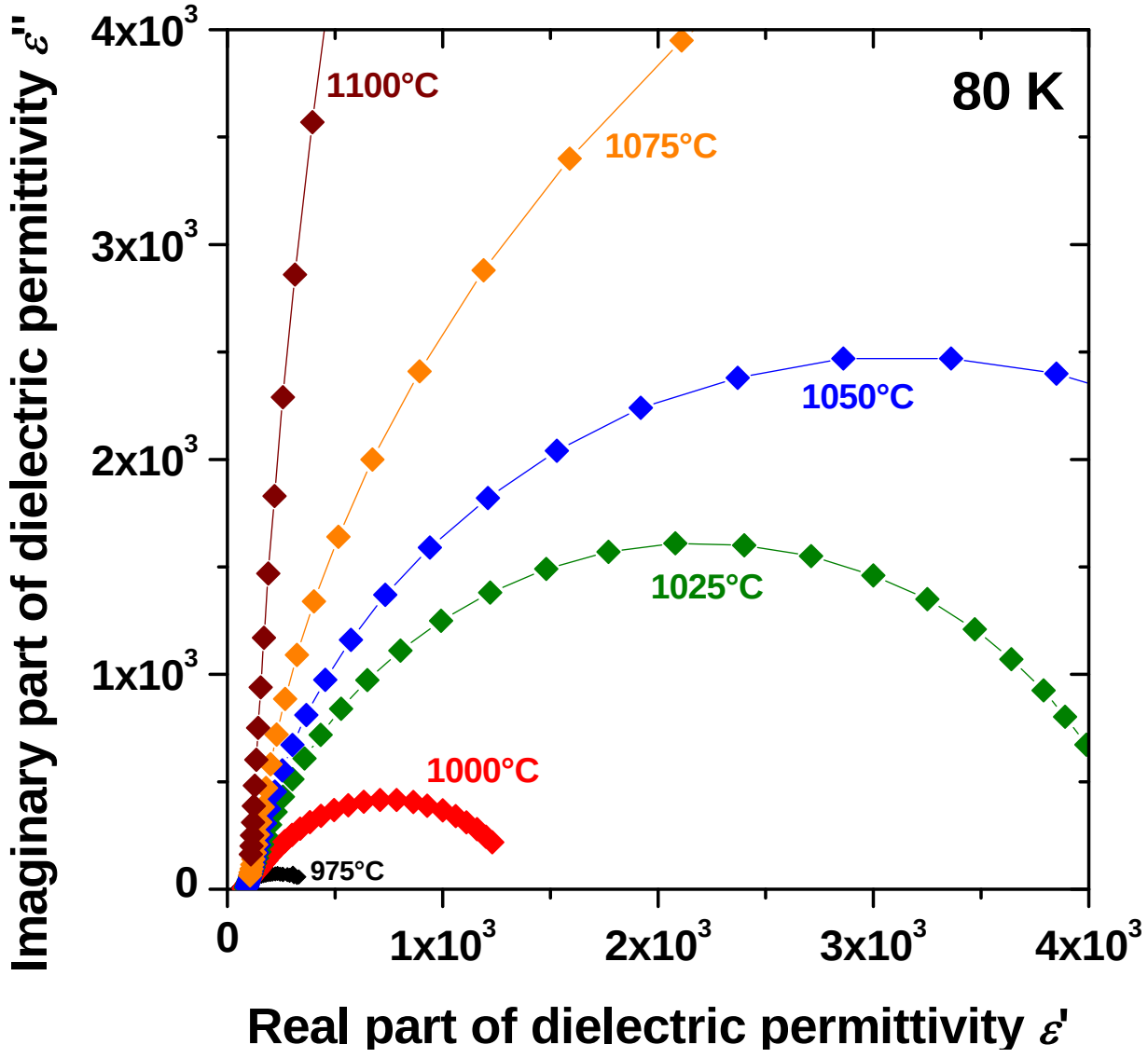

SOM Figure 1 Cole-Cole plots of ε" vs ε' for CCTO pellets sintered at different temperatures. The diameter of the semicircle is proportional to the GB permittivity. A strong increase of GB permittivity with T_S is observed.

In order to obtain ε_1 from ε_1* according to equation (SOM3) the GB permittivity ε_2 was determined from the low f plateau in plots of ε' vs f at 80 K (Fig.2 in the main text), where a large increase in ε_2 with T_S was detected. This trend was confirmed and analyzed in more detail

from plots of the imaginary part of the permittivity ε" vs the real part ε'. Such Cole-Cole plots presented in SOM Fig.1 display an ideal semicircle in the case of two parallel RC elements connected in series for ideal GB and bulk relaxations. For CCTO ceramics the GB and bulk resistance values always differ by at least 3 orders of magnitude. In this case, the low frequency *x*-axis (ε' axis) intercept is an excellent estimate for the GB permittivity ε_2, whereas the high frequency intercept corresponds to ε_1*. The size of the Cole-Cole semicircles increases with T_S (SOM Fig.1), which confirms the increase of GB permittivity with T_S mentioned in the main text. To summarize, the GB permittivity ε_2 was determined from the high ε' plateau at low *f* in plots of ε' vs *f*. Equation SOM3 was used to calculate ε_1 for each sample from those ε_2 values and from the low ε' plateau ε_1* at high *f* in ε' vs *f*. The calculated ε_1 values varied from ε_1* by + 14 % for T_S = 975 °C, and this deviation decreased to + 0.1 % for T_S = 1100 °C. The bulk resistivity ρ_1 was then determined from equation SOM2 using the corrected ε_1 values and the f_{max} values of the bulk dielectric relaxation peak determined from *M* " vs *f* plots.

The increase of bulk conductivity with increasing T_S was shown in Fig.3 in the main text. Such behavior could be confirmed from complex impedance plots of *Z*" vs *Z*' as shown in SOM Fig.2, where the diameter of the bulk semicircle displayed is proportional to the bulk resistivity ρ_1. In fact, two semicircles are displayed, which can be seen most clearly for the sample sintered at 1075 °C. At the higher frequency end an almost fully developed bulk semicircle appears near the origin of the plot, whereas a second larger semicircle appears at the lower frequency end. This second large semicircle represents the GB contribution, but is too large to be fully resolved on this scale, i.e. the GB resistance is large. In fact, the GB resistivity was overlaid by a non-ohmic electrode interface relaxation, which did not allow reliable extraction of GB resistivity values. For the 1100 °C sintered pellet the bulk semicircle near the origin is not fully developed and only

a non-zero intercept of the data on the real Z' axis is observed with only the onset of a small bulk semicircle. For 1025 °C and 1050 °C sintered ceramics only a fraction of the bulk semicircle can be displayed due to increased bulk resistivity. For 975 °C and 1000 °C sintered pellets only the onset of the bulk semicircle is shown, emphasizing the massive increase in bulk resistivity ρ_1 with decreasing T_S.

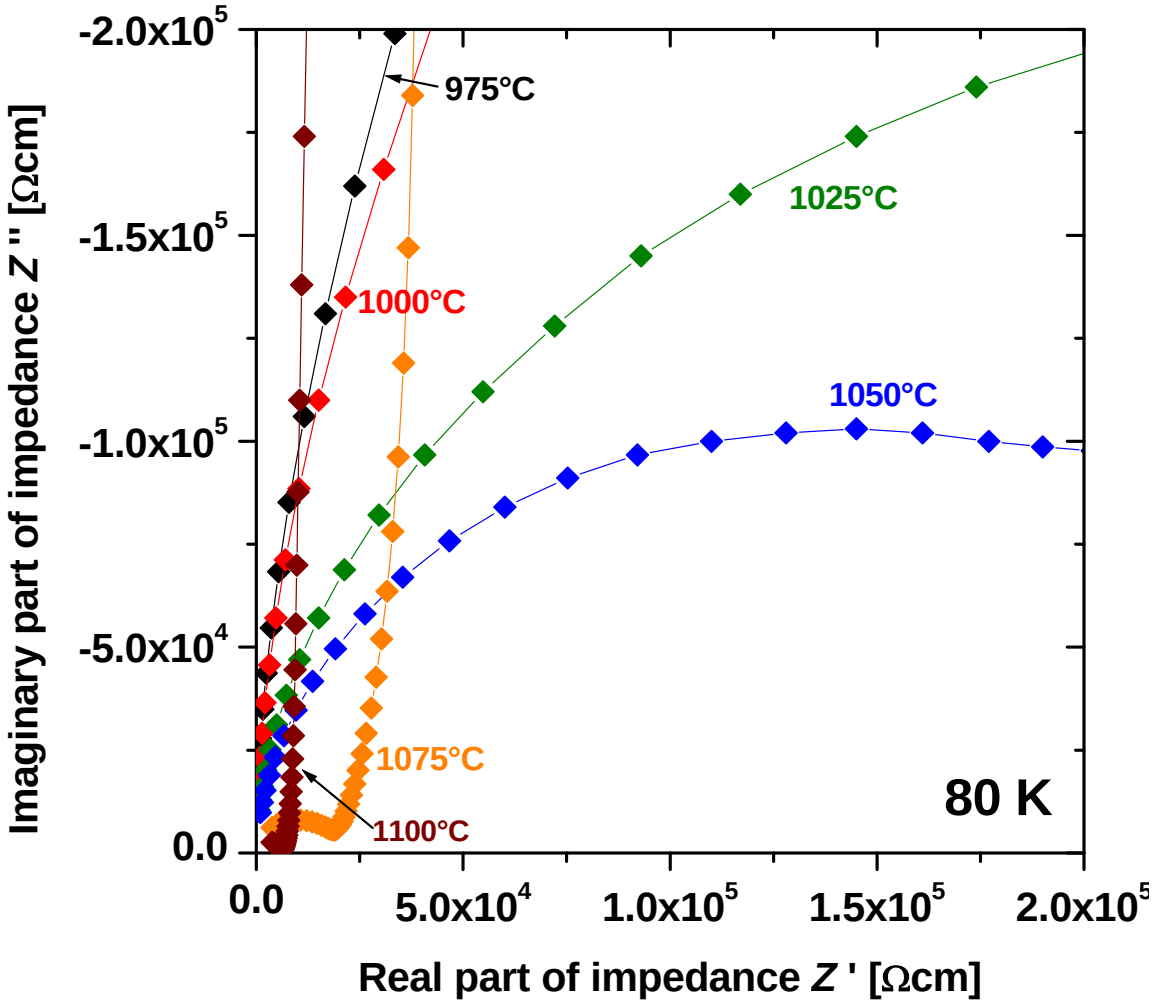

SOM Figure 2 Complex-plane plots of Z'' vs Z' for CCTO pellets sintered at different temperature. The diameter of the high f semicircle is proportional to the bulk resistivity. A large increase of bulk resistivity ρ_1 is observed with decreasing T_S.

II. Fabrication of CuTi and $CaTiO_3$ standards for quantitative EDAX analysis

To obtain quantitative EDAX results of Ca:Cu:Ti ratios from CCTO pellets, Cu:Ti and Ca:Ti standards were fabricated. An 1:1 CuTi alloy was produced from high purity Cu and Ti metals (99.98%) and 3 repeated rapid melting processes at ≈ 3000 °C in high vacuum for a few seconds were carried out to homogenize the alloy. The mass loss of the alloy in relation with the separated metals was in the range of 0.2 % and Cu- or Ti-loss was negligible. The alloy was analyzed quantitatively by SEM using the EDAX detector and the oxygen content was below the detection limit of the analyzer. Furthermore, no indication of Cu:Ti inhomogeneity was observed on all accessible length scales. A $CaTiO_3$ standard was prepared at 1150 °C from dried and intermixed precursors of $CaCO_3$ and TiO_2 reagents, pressed into a pellet and sintered in air at 1600 °C. EDAX analysis showed no evidence of Ca:Ti inhomogeneity on all accessible length scales. The metal ratios of the CuTi and $CaTiO_3$ standards were assumed to be 1:1 each, and were then measured by EDAX. Large area (≈ 1 × 1 mm) scans were carried out with each containing at least 2000 pixels over a period of ≈ 2 mins with a count rate of ≈ 5 k/sec. This analysis was repeated on 5 selected areas on each of the polished standard surfaces. The results showed good consistency and were averaged to correct the Ca:Cu:Ti ratios obtained from CCTO samples.

III. SEM microstructure analysis of sintered CCTO pellets

SOM Figure 3 shows SEM images collected with secondary electrons (left side) and backscattered electrons (right side) for CCTO pellets sintered at different temperatures, T_S. The image contrast in the secondary electron pictures (left) is mainly due to topographical contrast, whereas the image contrast in backscattered electron pictures (right) is mainly due to elemental contrast. Moderate grain growth is evident with increasing T_S.

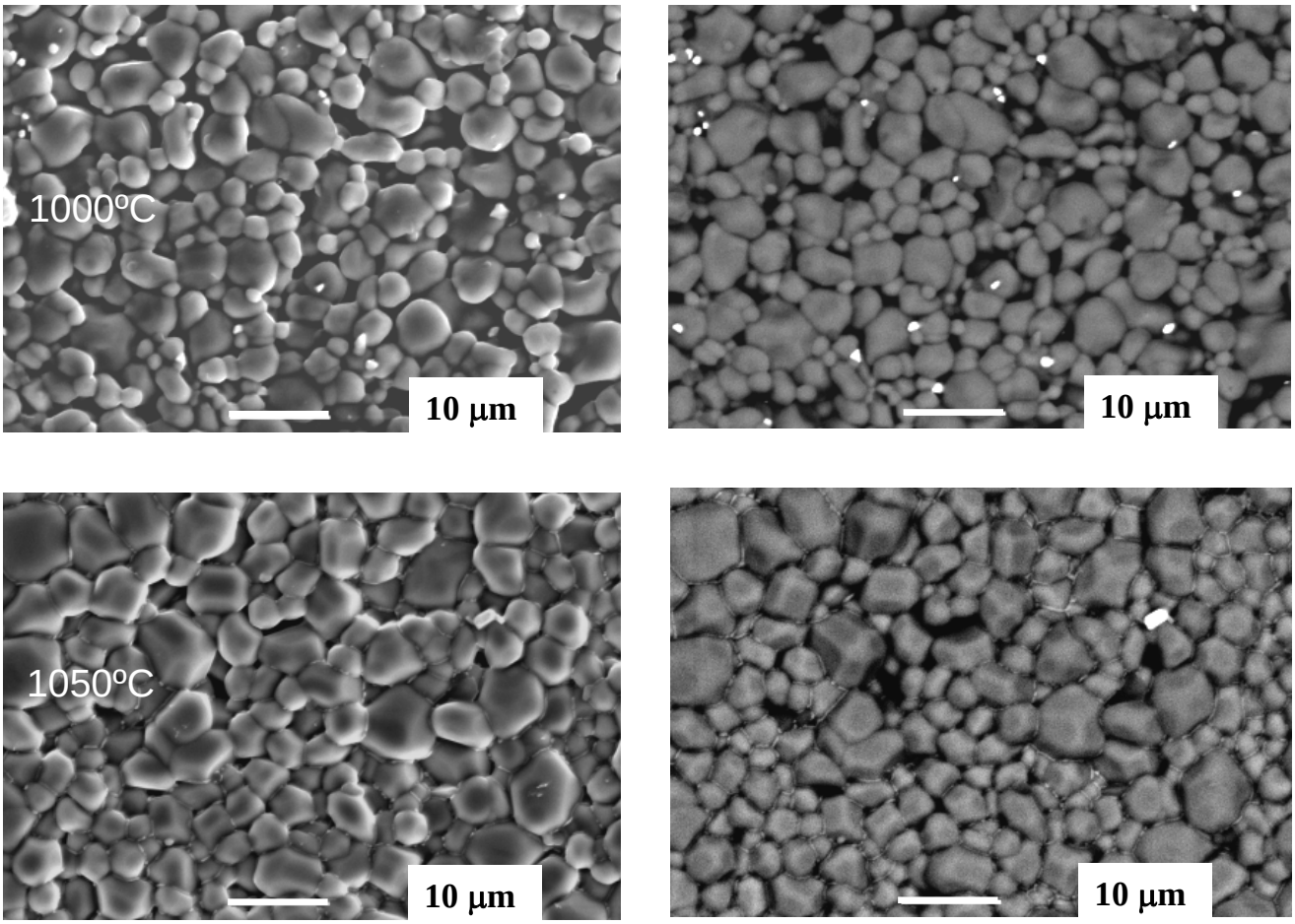

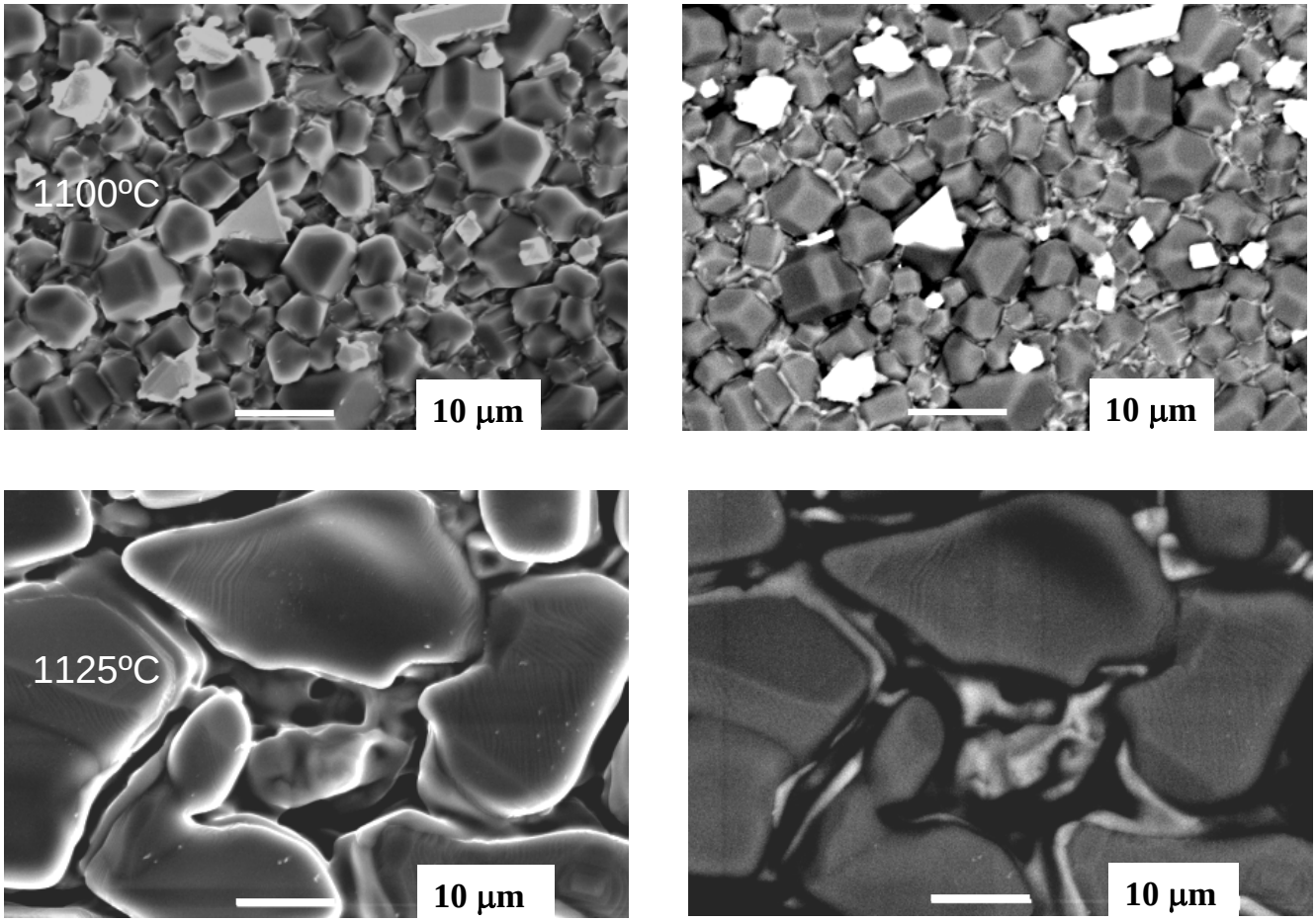

SOM Figure 3 SEM images collected with secondary electrons (left side) and backscattered electrons (right side) for CCTO pellets sintered at different temperatures, T_S. Moderate grain growth is evident with increasing T_S. At 1050 °C a Cu-rich phase segregates out and at 1125 °C CCTO decomposes accompanied by Cu volatilization.

A Cu-rich phase starts to segregate out of the CCTO ceramics at T_S = 1050 °C, which can be seen as a bright inter-granular phase in the backscattered electron image. A better account of this effect is given in the main text in Fig.5. The very bright spots in the backscattered electron image for the 1100 °C ceramic (SOM Figure 3) are Pt residues from the Pt foil on which the pellets

were sintered. At 1125 °C the CCTO phase decomposes. By using EDAX spot analysis on such a 1125 °C sintered pellet it was found that the large grains displayed in the SEM images are Ti-rich and may be associated with TiO_2. Furthermore, $CaTiO_3$ grains were indicated, but only very few CCTO grains and no Cu-rich phase could be detected. Such a phase composition was confirmed using XRD and decomposition of the CCTO phase and Cu volatilization was indicated.

Large area average EDAX measurements revealed considerable Cu-deficiency in the 1125 °C ceramic and Cu volatilization seems a plausible explanation. From the results presented here it seems clear that a Cu-rich phase first segregates out of the CCTO ceramic. This is clearly visible for T_S = 1050 °C or above. For T_S = 1125 °C, CCTO decomposes and a substantial Cu-loss indicates Cu volatilization, which is consistent with the thermal gravimetry results presented in the main text (Fig.7). The segregating Cu-rich phase exhibits high mobility because it accumulates at the surfaces of the ceramics and at higher temperatures a high volatility is indicated due to Cu-loss. The CCTO phase may be regarded as an open system where thermal energy provided by heating leads to segregation and volatilization of a Cu-rich phase prior to decomposition.

From the backscattered SEM images shown on the right hand side of SOM Figure 3 the mean grain sizes were determined by averaging the size of 220 randomly selected CCTO grains. SOM Figure 4 demonstrates a moderate grain growth with increasing T_S. The trend is approximately linear up to 1075 °C, whereas sintering at 1100 °C leads to an additional increase in grain size. The grain growth is accompanied by an increase in pellet density (also shown in SOM Figure 4) as expected for such densification sintering processes. The grain size distributions are shown in SOM Figure 5.

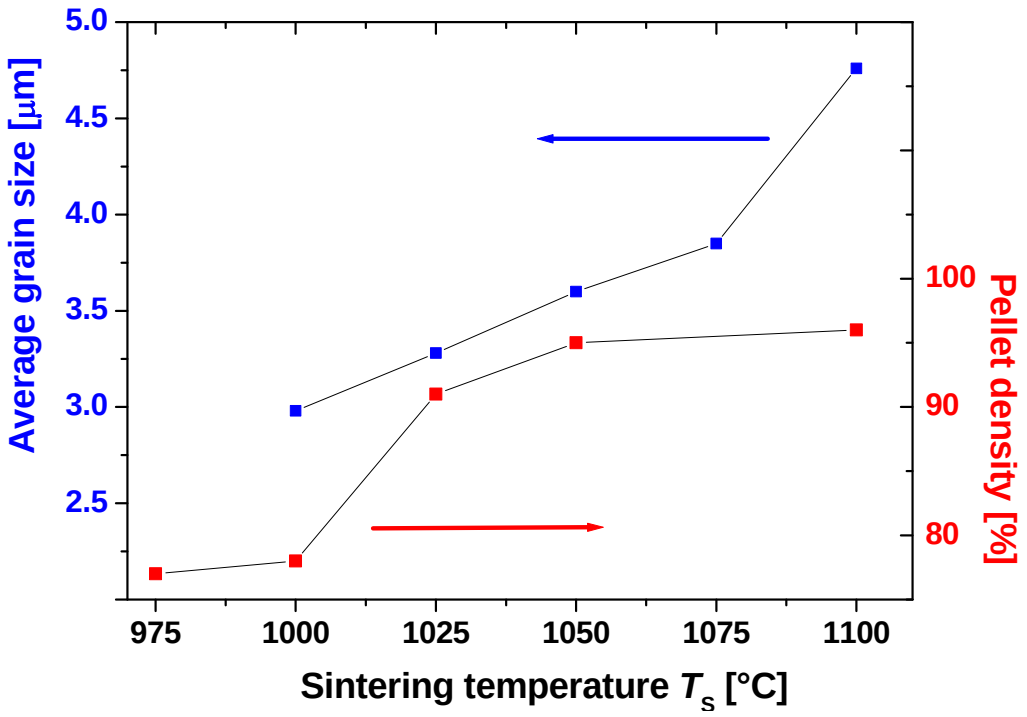

SOM Figure 4 Average grain size of sintered pellets vs sintering temperature T_S (left y-axis), and pellet density vs T_S (right y-axis).

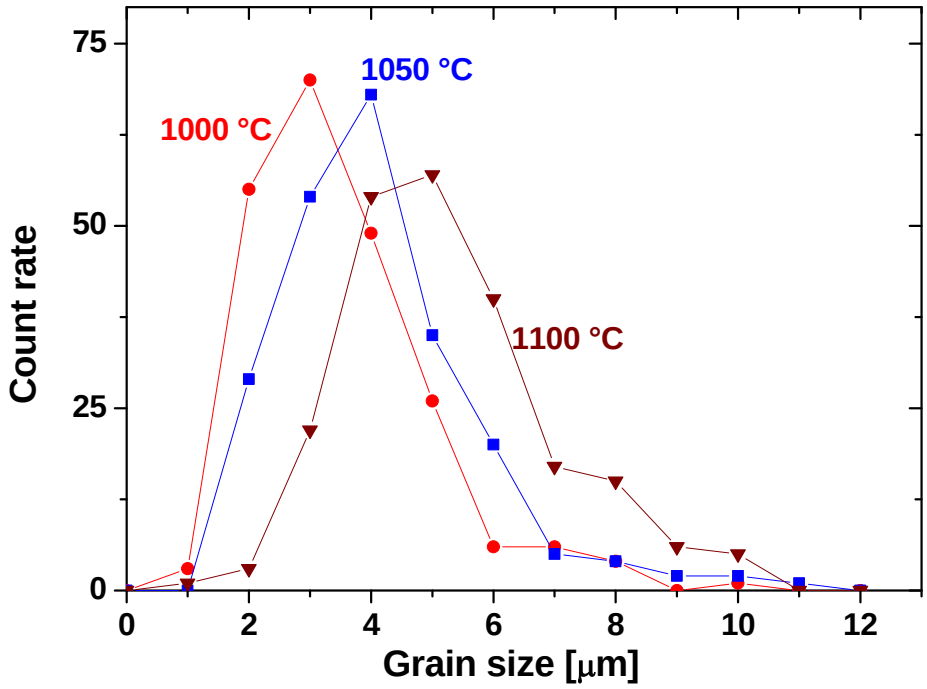

SOM Figure 5 Grain size distribution for pellets sintered at different temperature T_S as indicated.

Supporting Online Materials References

1. Barsukov E, Macdonald J, *Impedance Spectroscopy: Theory, Experiment and Applications*. John Wiley & Sons Inc.: Hoboken, 2005.

2. Irvine JTS, Sinclair DC, West AR. *Adv Mater* 1990;**2**:132.

3. Schmidt R, Impedance Spectroscopy of Electroceramics. In *Ceramic Materials Research Trends*, Lin PB, Ed. Novascience Publishers: Hauppauge, 2007; p 321.

4. Lunkenheimer P, Fichtl R, Ebbinghaus SG, Loidl A. *Phys Rev B* 2004;**70**:172102.

5. Schmidt R, Sinclair DC. *Chem Mater* 2010;**22**:6.